Demonstration of a Class E push-pull resonant inverter for MHz induction heating

Aunsborg, Thore Stig; Bidoggia, Benoît; Bro Duun, Sune; Kjærsgaard, Benjamin Futtrup; Meinert, Janus Dybdahl; Jørgensen, Asger Bjørn; Munk-Nielsen, Stig

Published in:
APEC 2023 - 38th Annual IEEE Applied Power Electronics Conference and Exposition

DOI (link to publication from Publisher):
10.1109/APEC43580.2023.10131354

Publication date:
2023

Document Version
Accepted author manuscript, peer reviewed version

Demonstration of a Class E push-pull resonant inverter for MHz induction heating

Thore Stig Aunsborg*, Benoît Bidoggia†, Sune Bro Duun†, Benjamin Futtrup Kjærsgaard*
Janus Dybdahl Meinert*, Asger Bjørn Jørgensen*, Stig Munk-Nielsen*
Email: {tsu,bfk,jdm,abj,smn}@energy.aau.dk, {beb,sdu}@gw-topsil.com
*Department of Energy, Aalborg University, Denmark †R&D Department, Topsil GlobalWafers, Denmark

***Abstract*—Industrial heating processes operating at frequencies of multiple MHz often have low efficiencies due to the use of vacuum-tube technology. This can be improved using inverters based on wide band gap materials, but requires special attention in topology selection to achieve high efficiency in a range of operating conditions. This paper investigates the merits of the Class E push-pull resonant inverter topology for MHz induction heating. A prototype SiC MOSFET power module is manufactured and experimentally validated in a Class E push-pull inverter system with a commercial induction heating load. The inverter is demonstrated up to a power of 5 kW with high efficiency, verifying the performance of the approach for industrial RF heating systems.**

***Index Terms*—Resonant inverter, wide bandgap devices, soft-switching, induction heating**

I. Introduction

Common industrial heating processes at RF frequencies, such as dielectric heating for curing and drying, or induction heating processes for zone refining of silicon, are limited in their efficiency due to the use of vacuum tube oscillators that are typically only 60-70% efficient [1]–[3]. This can be drastically improved by replacing the tubes with solid state devices, in particular by taking advantage of wide band gap (WBG) technology [4], [5]. In a variety of applications, DC-AC inverters (or equivalently, switched-mode amplifiers) operating with high efficiency at MHz frequencies and several kW have been demonstrated [6]–[9]. These advancements hold promise for further utilization of WBG devices for RF inverters in heating applications by pushing towards higher operating frequency, power delivery, and efficiency of the inverters. In this paper, an approach to this is demonstrated using a resonant inverter system for MHz induction heating based on the Class E push-pull topology. First, the operational principles and merits of the topology are described, after which an experimental setup for validating the performance and efficiency of the system is presented. Lastly, the results of operation with a MHz induction heating load are presented and discussed.

II. Topology description

Several topologies of resonant inverters have been applied to induction heating processes, including both current- and voltage source bridge inverters, single switch inverters, and inverters with multiple load elements such as LLC [10], [11]. For low impedance induction heating loads as well as high frequency operation, the Class E push-pull topology investigated here is attractive for several reasons. These include constant current drawn from the DC source, and the use of a parallel resonant tank which allows for current gain as well as inherent work coil short circuit capability [9], [12], [13]. In addition, the switch gates are driven with reference to the same potential and, as shown in red and green in Fig. 1(a), the circuit can be made in a way that incorporates the switch output capacitance and the circuit stray inductance in a secondary resonance loop that shapes the voltage across the switches to achieve zero voltage switching (ZVS) under a wide range of load frequency variation.

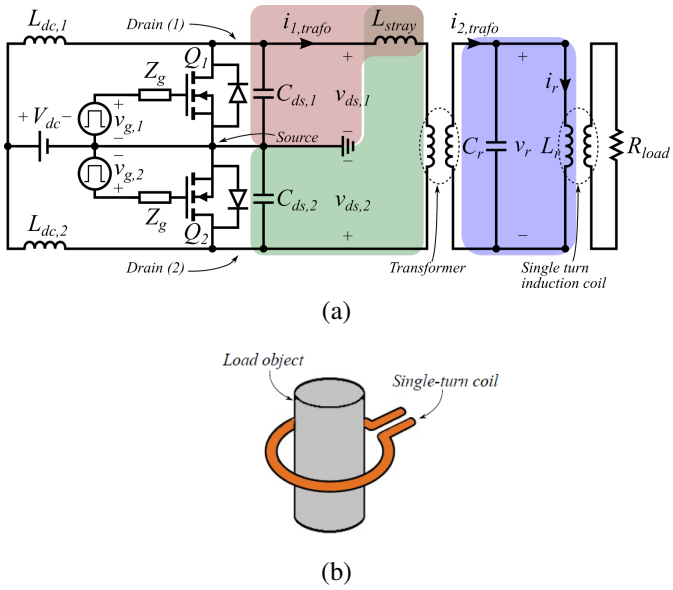

Fig. 1. a) schematic of the Class E push-pull inverter illustrating the resonant current paths and b) single-turn coil used for high-current induction heating [14].

This is seen in the circuit waveforms for the inverter operated at the tank resonance frequency in Fig. 2; the diode conduction provides inherent zero voltage switching at turn-on within the time interval T_{B} allowing for clean switching waveforms at MHz frequencies and reduced sensitivity to inaccuracies in the control timing. The leakage inductance of the transformer, which is the main parasitic inductive element, functions as a simple inductance between two phase-shifted

voltage sources (the inverter stage and the resonant tank).

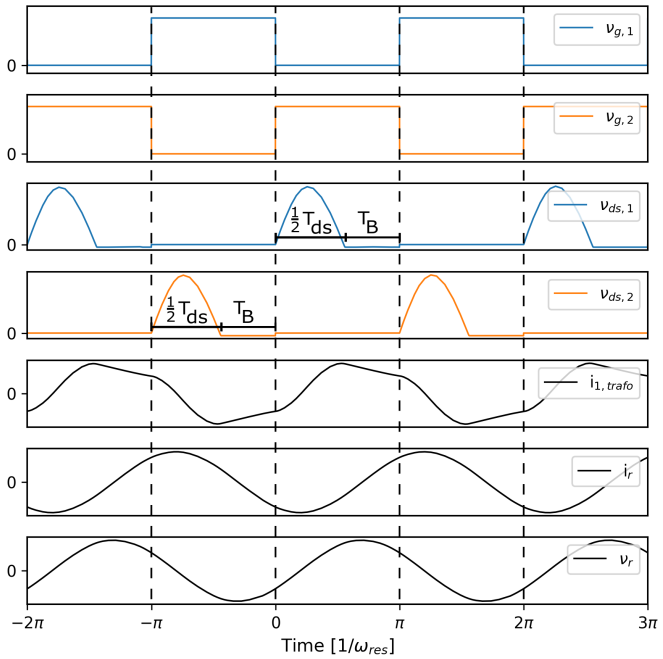

Fig. 2. Simulated voltage and current waveforms of the Class E push-pull inverter. One tank resonance period is $T_{\mathrm{res}} = T_{\mathrm{ds}} + 2T_{\mathrm{B}}$.

To maximize power transfer to the parallel resonance tank, the switching frequency should be kept relatively close to the tank resonance frequency. The requirement for soft switching of the MOSFETs is that the drain-source resonance voltage is in the negative half cycle at turn on. Thus, by letting the switching frequency follow the resonance frequency during operation, soft switching is achieved in the frequency range

$$f_{\mathrm{res}} = f_{\mathrm{sw}} < f_{\mathrm{ds}} < 2f_{\mathrm{res}} \tag{1}$$

However, the main drawback of the topology, as with the classic single ended Class E amplifier, is the relatively poor switch utilization factor c_{pmr} due to high voltage voltage across the switch given by [15]

$$c_{\mathrm{pmr}} = \frac{\eta_{\mathrm{D}} V_{\mathrm{dc}} I_{\mathrm{dc}}}{N V_{\mathrm{ds,p}} I_{\mathrm{ds,rms}}} \tag{2}$$

where η_{D} is the drain efficiency of the amplifier, V_{dc} and I_{dc} are the input voltage and current, respectively, N is the number of utilized switches, $V_{\mathrm{ds,p}}$ is the peak switch voltage, and $I_{\mathrm{ds,rms}}$ is the switch RMS current. To achieve both zero voltage and zero voltage derivative switching (ZVDS), the Class E amplifier has $V_{\mathrm{ds,p}}/V_{\mathrm{dc}} = 3.56$ for the ideal case, and generally larger still when considering the non-linear switch parasitic capacitance [16], [17]. Several alternatives or modifications to the Class E topology, such as the Class F or Class Φ_2, achieve higher c_{pmr} by shaping the harmonic content of the voltage across the switches using additional resonant networks, at the expense of increased complexity [15], [18], [19]. The presented embodiment of the Class E amplifier does not aim to achieve ZVDS, but instead relies on the drain-source resonance loop to achieve ZVS over a wide resonance frequency range given by (1). This narrows the drain-source voltage, which from the volt-second balance of the DC chokes further increases the ratio $V_{\mathrm{ds,p}}/V_{\mathrm{dc}}$, thus lowering c_{pmr} [14]. The topology investigated here is thus mainly attractive in applications where robustness towards frequency variation of the load is valued over switch utilization.

Considering the practical implementation of the inverter, this topology can achieve high efficiency in particular thanks to the incorporation of both capacitive and inductive parasitics. The high frequency of the application considered here means that the transformer leakage inductance is easily used as the primary inductive element in the drain-source loop, which must then be matched with the switch parasitic capacitance, constraining the values of practical elements in this resonance loop.

III. Design and Components

A prototype inverter system using a Class E push-pull topology for MHz induction heating was manufactured and tested. In addition to providing the normal functions of galvanic isolation and impedance matching (while maintaining high coupling factor), the transformer in this topology must also provide an adequate leakage inductance seen from the primary side to yield the desired drain-source resonance frequency. Because of the high frequency and the relatively low desired inductance values, an air-core transformer was designed and built as shown in Fig. 3. A spiral layout of flat ribbon windings is used to provide a coupling factor $k > 0.7$ and the desired electrical parameters while maintaining high voltage isolation and good thermal performance.

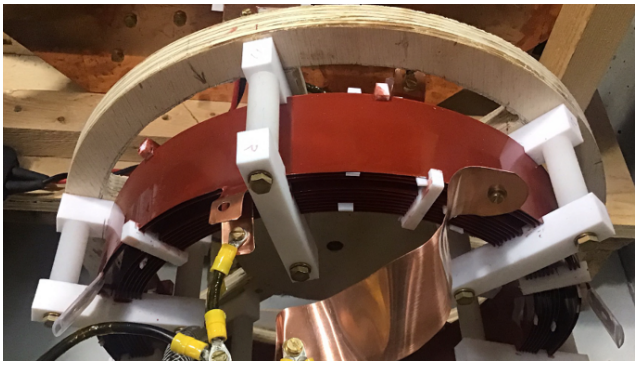

Fig. 3. Picure of the constructed transformer with tabs for adjustment of the primary, secondary, and leakage inductances.

A custom integrated power module was designed and built for the inverter as shown in Fig. 4. Each switch is made from two 1700 V SiC MOSFETs in a symmetric layout with auxiliary source connections. High voltage capacitors C_{cap} are added in parallel to the MOSFETs to achieve the desired f_{ds} and reduce its voltage dependency, particularly at higher voltages. For simplicity of the driving circuit and

high operating frequency flexibility, a hard switched gate drive topology is chosen. However, driving the input capacitance of the paralleled MOSFETs at multiple MHz requires the driver IC to source and sink large peak currents. Thus, the driver ICs are integrated in the power module to improve the thermal performance and achieve high switching speed with a small gate switching loop. An advantage of the inverter topology is that neither the input nor the output of the module is sensitive to stray inductance, leading to a large degree of flexibility in the module design.

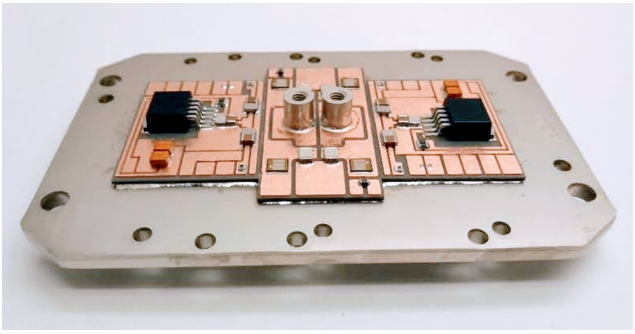

Fig. 4. Picture of the power module for the inverter before wire bonding, terminal welding, and encapsulation.

The power module, DC chokes, and high-frequency transformer are connected by cables on the primary side, while the secondary side is connected to the parallel resonant tank using a busbar structure, as shown in Fig. 5. The resonant tank is comprised of a flat single turn inductor coil with a steel block load connected to a 40 nF vacuum capacitor bank [9], yielding the resonance frequency $f_{\mathrm{res}} \approx 2.4$ MHz. The components of the inverter system are summarized in Table I.

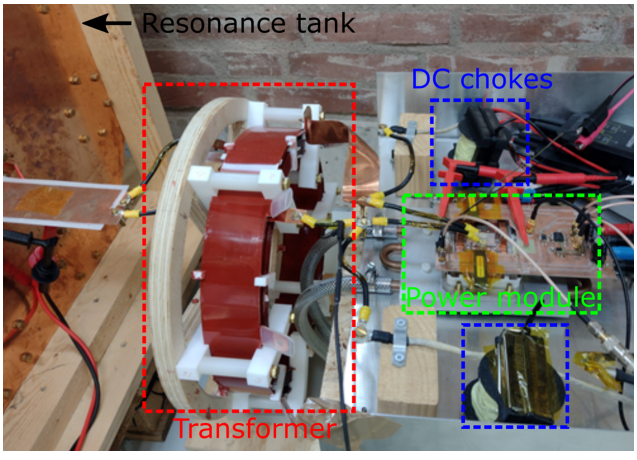

Fig. 5. Picture of the experimental setup, with wires and busbars connecting the discrete elements of the inverters.

As the parasitic MOSFET output capacitance is highly voltage dependent, it is important to evaluate it at the operating voltage to ensure that drain-source resonance frequency is within the desired range. The capacitance at a given voltage

TABLE I
PROTOTYPE COMPONENT VALUES.

Component	Value	Implementation
S1, S2	$R_{\mathrm{ds,on}} = 80$ mΩ $C_{\mathrm{oss}} = 105$ pF @ 1000 V	4x CPM2-1700-0080B
Gate drivers	$\nu_{\mathrm{g}} = -4$ V/ + 18 V	2x IXDN614YI
Module capacitors	$C_{\mathrm{cap}} = 470$ pF	4x C1812X471JGGACTU
Transformer	$n = 2:7$, $L_{\mathrm{p}}^{\sigma} = 1.0$ uH $L_{\mu} = 1.1$ uH	Spiral windings, air-core
DC chokes	$L_{\mathrm{dc}} = 49$ uH	2x EMS-0653327-060 powder cores, 15 windings

level is found as the charge-equivalent output capacitance [20]

$$C_{\mathrm{oss,eq}} = \frac{\int_0^{V_{\mathrm{ds}}} C_{\mathrm{oss}}(\nu)\mathrm{d}\nu}{V_{\mathrm{ds}}} \tag{3}$$

Combined with the fixed capacitance from the module capacitors, and by ignoring other parasitic capacitances from module and transformer and small stray inductances, the drain-source resonance frequency is found from

$$f_{\mathrm{ds}} \approx \frac{1}{2\pi\sqrt{2(C_{\mathrm{oss,eq}} + C_{\mathrm{cap}})L_{\mathrm{p}}^{\sigma}}} \tag{4}$$

The impedance seen from the module terminals is seen in Fig. 6, where the tank resonance is observed at 2.4 MHz. This is compared to a simple SPICE model of the inverter, including switch parasitics and parameters from table I. From the datasheet of the MOSFETs $C_{\mathrm{oss}}(0\mathrm{V}) \approx 2.25$ nF, yielding a total switch capacitance of $2(C_{\mathrm{oss}}(0\mathrm{V}) + C_{\mathrm{cap}}) = 5.44$ nF. Since the switch capacitances are in series in this measurement

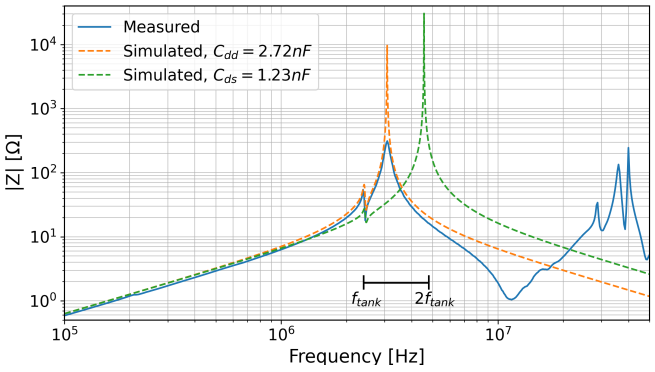

Fig. 6. Load impedances measured and simulated from the power module output terminals. The usable f_{ds} operation range for this load configuration is highlighted.

configuration, the apparent drain-drain capacitance is 2.72 nF, which fits well with the measured impedance result. The green dotted line shows the estimated impedance from drain to source for each switch assuming a peak voltage of 800 V

according to (3) and (4). From this, the drain-source capacitance becomes $C_{\mathrm{ds}} \approx 1.23$ nF resulting in $f_{\mathrm{ds}} = 4.56$ MHz, which is within the ZVS operating range determined by (1).

IV. Experimental results

The measurements setup consists of two HDO6034 oscilloscopes, where the high voltage signal of the resonant tank and the MOSFET drains are measured using HVD3605A and HVD3206 differential probes, respectively. The transformer input and resonant tank currents are measured with PEM CWT Rogowski current transducers. The resonant inductor, load, and power module are water cooled with individual cooling loops, allowing the dissipated power and efficiency of each element to be estimated from calorimetric measurements. The gate- and drain voltage waveforms of the induction heating setup when operated close to the tank resonance frequency are shown in Fig. 7. In contrast to many other inverter types, the body diodes of the MOSFETs are carrying current during a significant fraction of the switching period, since f_{ds} may be significantly larger than f_{res}. The forward voltage of the MOSFET body diode is around 4 V, which means this is potentially a detriment to the inverter efficiency. However, as the drain voltage is shaped by drain-source resonance, there is no switching loss penalty for increasing the duty cycle to turn on the MOSFETs shortly following the start of diode conduction. This insensitivity of the turn-on timing greatly simplifies the operation of the inverter and makes the topology attractive for simple frequency tracking control implementations.

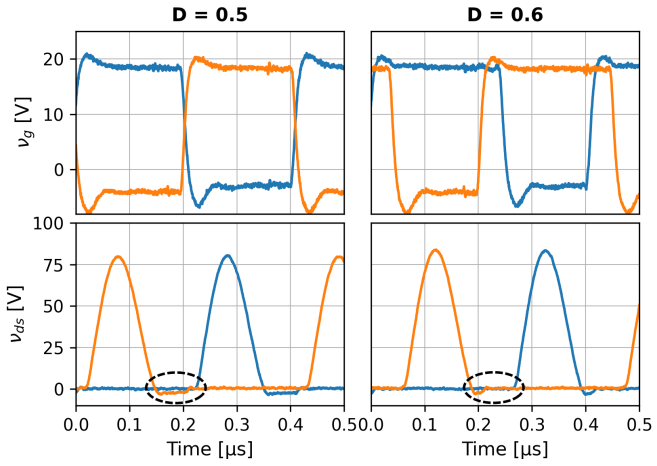

Fig. 7. Measured voltage waveforms of the inverter under variation of the duty cycle to reduce diode active time.

The drain-source resonance frequency variation with transistor voltage is shown in Fig. 8. For very low voltages, (1) is not necessarily satisfied due to the large C_{oss}, but complete soft switching is not required for safe operation at low power. At higher voltage, the static capacitance dominates the MOSFET capacitance, and the resonance frequency variation with voltage is reduced.

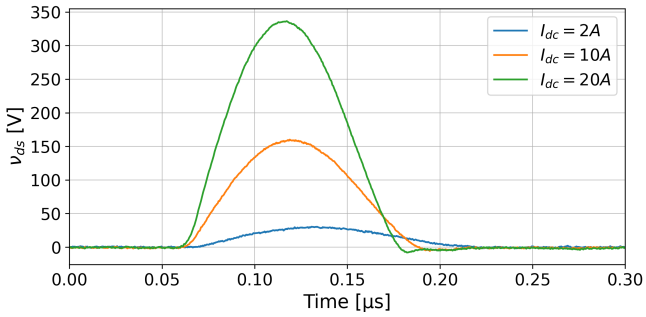

Fig. 8. Measured drain-source voltage for varying input current showing the voltage dependency of the drain-source resonance frequency.

The measured resonance tank voltage and currents are shown in Fig. 9. The apparent load resistance is around 1.4 Ω, showing that significant current levels are required for the loosely coupled load. The resonant tank current is not measured at higher voltage levels to have sufficient margin to the voltage limits for the current probe.

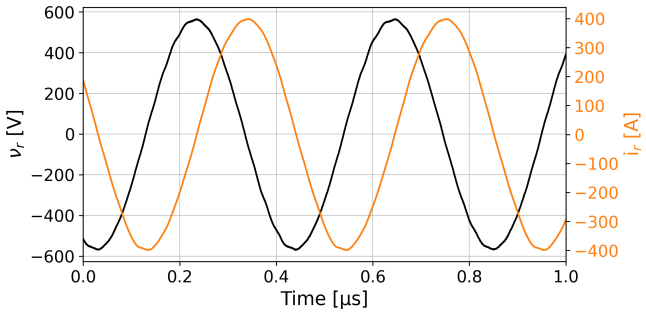

Fig. 9. Measured resonant tank voltage and current at 1.6 kW input power.

Fig. 10 shows the measured waveforms for a continuous input power of 5 kW. The inherent inclusion of parasitic parameters in the resonance loops allows for the clean voltage and current waveforms presented here, avoiding unwanted resonances even at high voltage and current levels. The transformer current was measured with a Rogowski probe and thus has a small delay that is apparent as a slight phase shift between the transistor voltage and the transformer input current. For the peak drain voltage 800 V, the voltage waveform width is $\frac{1}{2}T_{\mathrm{ds}} = 112$ ns, corresponding to $f_{\mathrm{ds}} = 4.46$ MHz, closely matching the predictions from Fig. 6. Using the equivalent resistance value of 1.4 Ω in this load configuration and $V_{\mathrm{r,rms}} = 713$ V at this operating point, an estimated reactive power of 363 kVA is oscillating in the resonance tank.

The efficiency was measured calorimetrically, where the inverter has been operated continuously for 3 minutes to make sure the cooling water temperature had stabilized in each cooling loop. For an input power of 4.07 kW, an output power of 3.31 kW was dissipated in the resonant coil and load, while 0.21 kW was dissipated in the power module, yielding a system efficiency of 81% and a power module operational

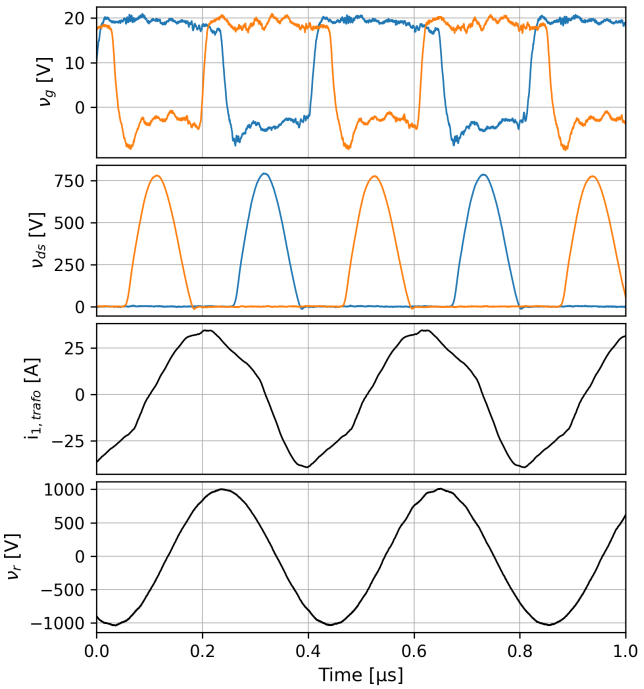

Fig. 10. Measured voltages and currents of the inverter at 5kW input power.

efficiency of 94%. The system efficiency is likely to be improved through optimization of the operational parameters and designs of the auxiliary components, while the power module efficiency demonstrates the applicability of the topology for RF heating purposes.

V. Conclusions and Future Work

This paper demonstrates a Class E push-pull resonant inverter for industrial MHz induction heating. The merits of the inverter topology in this application have been presented, and considerations for practical implementations of the inverter blocks have been discussed. A prototype inverter utilizing a 1700 V SiC MOSFET power module and a custom designed transformer has been demonstrated using a relevant industrial load. The system performance has been showcased under different operating conditions up to an input power of 5 kW, and an efficiency of 81% for the whole system and 94% for the power module has been calorimetrically measured. The presented design paradigm demonstrates the applicability of the Class E push-pull inverter for implementations of industrial MHz heating systems. Further studies will focus on improving these parameters and designs to increase the efficiency and scale up the power handling capability of the inverter.

References

[1] Gupta, A., Arondekar, Y., Ravindranath, S.V.G.G., Krishnaswamy, H., Jagatap, B.N.: 'A 13.56 MHz high power and high efficiency RF source', *IEEE MTT-S International Microwave Symposium Digest*, 2013, pp. 1–4

[2] Richardson Electronics. 'Dielectric heating', . Available from: https://www.relltubes.com/filebase/en/src/Brochure/DielectricBrochure_FINAL_LR_051412.pdf

[3] Mühlbauer, A. 'Innovative Induction Melting Technologies: A Historical Review'. In: Modelling for Material Processing, 2006.

[4] Guo, S., Zhang, L., Lei, Y., Li, X., Xue, F., Yu, W., et al.: '3.38 Mhz operation of 1.2kV SiC MOSFET with integrated ultra-fast gate drive', *IEEE Workshop on Wide Bandgap Power Devices and Applications*, 2015, pp. 390–395

[5] Aunsborg, T.S., Duun, S.B., Uhrenfeldt, C., Munk.Nielsen, S. 'Challenges and opportunities in the utilization of WBG devices for efficient MHz power generation'. In: Proceedings of IECON, 2019. pp. 5107–5113

[6] Denk, F., Haehre, K., Simon, C., Eizaguirre, S., Heidinger, M., Kling, R., et al. '25 kW high power resonant inverter operating at 2.5 MHz based on SMD Phase-Leg Modules'. In: PCIM. Power Conversion and Intelligent Motion Conference, 2018.

[7] Choi, J., Tsukiyama, D., Rivas, J. 'Comparison of SiC and eGaN devices in a 6.78 MHz 2.2 kW resonant inverter for wireless power transfer'. In: IEEE Energy Conversion Congress and Exposition (ECCE), 2016. pp. 1–6

[8] Lucía, O., Sarnago, H., Burdío, J.M. 'Design of power converters for induction heating applications taking advantage of wide-bandgap semiconductors'. In: COMPEL - The international journal for computation and mathematics in electricaland electronic engineering. vol. 36, 2017. pp. 483–488

[9] Aunsborg, T.S., Duun, S.B., Munk.Nielsen, S., Uhrenfeldt, C.: 'Development of a current source resonant inverter for high current MHz induction heating', *IET Power Electronics*, 2022, **15**, pp. 1–10

[10] Dede, E.J., Jordan, J., Esteve, V. 'State-of-the Art and Future Trends in Transistorised Inverters for Induction Heating Applications'. In: Proceedings of the Fifth IEEE International Caracas Conference on Devices, Circuits and Systems, 2004. pp. 204–211

[11] Lucia, O., Maussion, P., Dede, E., Burdio, J.M.: 'Induction Heating Technology and its Applications: Past Developments, Current Technology, and Future Challenges', *IEEE Transactions on Industrial Electronics*, 2013, **61**, (5)

[12] Dede, E.J., Jordan, J., Linares, J.A., Gonzalez, J.V., Esteve, V., Ramirez, D., et al. 'On the design of medium and high power current fed inverters for induction heating'. In: IEEE Industry Applications Society Annual Meeting, 1991. pp. 1047–1053

[13] Kazimierczuk, M.K.: 'Current-Source Parallel-Resonant DC/AC Inverter with Transformer', *IEEE Transactions on Power Electronics*, 1996, **11**, (2), pp. 275–284

[14] Meinert, J.D., Kjaersgaard, B.F., Aunsborg, T.S., Duun, S.B., Joergensen, A.B., Munk.Nielsen, S. 'Class-E Push-Pull Resonance Converter with Load Variation Robustness for Industrial Induction Heating'. In: 24th European Conference on Power Electronics and Applications (EPE'22 ECCE Europe), 2022. pp. 1–8

[15] Kaczmarczyk, Z.: 'High-Efficiency Class E, EF_2, and E/F_3 Inverters', *IEEE Transactions on Industrial Electronics*, 2006, **53**, (5), pp. 1584–1593

[16] Suetsugu, T., Kazimierczuk, M.K.: 'Comparison of class-E amplifier with nonlinear and linear shunt capacitance', *IEEE Transactions on Circuits and Systems I: Fundamental Theory and Applications*, 2003, **50**, (8), pp. 1089–1097

[17] Hayati, M., Roshani, S., Kazimierczuk, M.K., Sekiya, H.: 'A Class-E Power Amplifier Design Considering MOSFET Nonlinear Drain-to-Source and Nonlinear Gate-to-Drain Capacitances at Any Grading Coefficient', *IEEE Transactions on Power Electronics*, 2016, **31**, (11), pp. 7770–7779

[18] Rivas, J.M., Han, Y., Leitermann, O., Sagneri, A., Perreault, D.J.: 'A High-Frequency Resonant Inverter Topology with Low Voltage Stress', *IEEE Transactions on Power Electronics*, 2008, **23**, (4), pp. 1759–1771

[19] Gu, L., Zulauf, G., Zhang, Z., Chakraborty, S., Rivas.Davila, J.: 'Push–Pull Class Φ_2 RF Power Amplifier', *IEEE Transactions on Power Electronics*, 2020, **35**, (10), pp. 10515–10531

[20] Kasper, M., Burkart, R.M., Deboy, G., Kolar, J.W.: 'ZVS of Power MOSFETs revisited', *IEEE Transactions on Power Electronics*, 2016, **31**, (12), pp. 8063–8067